nature communications

Article

https://doi.org/10.1038/s41467-024-52068-0

# Protein kinase N promotes cardiac fibrosis in heart failure by fibroblast-to-myofibroblast conversion

Received: 13 December 2023

Accepted: 26 August 2024

Published online: 12 September 2024

Check for updates

Satoya Yoshida[1], Tatsuya Yoshida[1], Kohei Inukai[1], Katsuhiro Kato[1], Yoshimitsu Yura[1], Tomoki Hattori[1], Atsushi Enomoto[2], Koji Ohashi[3], Takahiro Okumura[1], Noriyuki Ouchi[3], Haruya Kawase[1,4], Nina Wettschureck[4], Stefan Offermanns[4], Toyoaki Murohara[1] & Mikito Takefuji[1]

Chronic fibrotic tissue disrupts various organ functions. Despite significant advances in therapies, mortality and morbidity due to heart failure remain high, resulting in poor quality of life. Beyond the cardiomyocyte-centric view of heart failure, it is now accepted that alterations in the interstitial extracellular matrix (ECM) also play a major role in the development of heart failure. Here, we show that protein kinase N (PKN) is expressed in cardiac fibroblasts. Furthermore, PKN mediates the conversion of fibroblasts into myofibroblasts, which plays a central role in secreting large amounts of ECM proteins via p38 phosphorylation signaling. Fibroblast-specific deletion of PKN led to a reduction of myocardial fibrotic changes and cardiac dysfunction in mice models of ischemia-reperfusion or heart failure with preserved ejection fraction. Our results indicate that PKN is a therapeutic target for cardiac fibrosis in heart failure.

Fibrosis is defined as the overgrowth, hardening, and/or scarring of various tissues and attributed to excess deposition of extracellular matrix (ECM) components[1]. It results from chronic inflammatory reactions induced by various stimuli in several organs[2,3]. Fibrosis is not a disease; however, chronic fibrotic tissue disrupts various organ functions, and it accounts for approximately half of all deaths in the developed world[4].

Heart failure is a global pandemic with increasing prevalence[5]. Furthermore, severity of cardiac fibrosis is correlated with progression of heart failure[6,7]. Myocardial infarction (MI), a typical example of cardiac fibrosis, is the most common cardiovascular disease that leads to heart failure[8]. Cardiomyocytes undergo apoptosis within hours to days due to ischemia-hypoxia, forming fibrotic tissues to replace the loss of architectural integrity[9]. Fibrosis is a pivotal process in preventing ventricular wall rupture after MI. However, chronic fibrosis, the expansion of fibrosis in cardiac areas remote to the infarction, leads to altered chamber compliance and increased ventricular stiffness, thereby compromising cardiac output. Myocardial fibrosis is associated with the subsequent hospitalization and death of patients with non-infarcted heart failure[6]. Recently, heart failure with preserved ejection fraction (HFpEF) has been classified as a subtype of heart failure with ventricular stiffness[10]. Compared with controls, patients with HFpEF have severe cardiac fibrosis[11]. However, although HFpEF is becoming the most common form of heart failure, its pathophysiologic mechanisms remain unclear[12].

Cardiac fibroblasts play essential roles in cardiac fibrosis by depositing collagens and other ECM components in response to pathological stimuli[13]. In the resting state, fibroblasts are incapable of producing significant amounts of ECM proteins[14]. However, they undergo conversion to myofibroblasts in infarcted and stressed hearts.

[1]Department of Cardiology, Nagoya University School of Medicine, Nagoya, Japan. [2]Department of Pathology, Nagoya University School of Medicine, Nagoya, Japan. [3]Department of Molecular Medicine and Cardiology, Nagoya University School of Medicine, Nagoya, Japan. [4]Department of Pharmacology, Max Planck Institute for Heart and Lung Research, Bad Nauheim, Germany. e-mail: takefuji@med.nagoya-u.ac.jp

Myofibroblasts secrete large amounts of ECM proteins and increase contractile filaments, such as α-smooth muscle actin (αSMA). Transforming growth factor-β (TGF-β) is a central cytokine involved in fibroblast activation and a therapeutic target for preventing or slowing fibrosis[15]. TGF-β inhibitors have not been used as a therapeutic medicine because TGF-β inhibition in regulatory T cells can exacerbate autoimmune disease[16]. Understanding how to harness the beneficial aspects of immunity and to slow maladaptive fibrosis is crucial to design effective treatments for fibrotic disease.

Additionally, other signaling cascades, including the small GTPase RHOA, have been implicated in cardiac fibroblast activation[17]. Protein kinase N (PKN), an effector protein kinase of RHOA, belongs to the cAMP-dependent, cGMP-dependent, and protein kinase C (AGC) kinase family[18–20]. RHOA and other RHOA-mediated signaling proteins play crucial physiological and pathological roles in cardiovascular diseases[21]. Recent in vivo analyses have shown that PKN physiologically contributes to the vascular tone of hypertension[22]. Moreover, PKN pathologically contributes to cardiac hypertrophy leading to heart failure[23] and tumor invasion of pancreatic cancer[24]. However, the role of PKN in fibrosis remains unclear. Here, we investigated whether PKN1/2 in cardiac fibroblasts could mediate cardiac fibrosis in various mouse models of heart failure.

## Results

### PKN1 and PKN2 were expressed in cardiac fibroblasts

There are three isoforms of PKN (PKN1, PKN2, and PKN3) in mammalian cells[25]. To examine the expressions of *PKN1, PKN2, and PKN3* in human cardiac cells, we analyzed publicly available single-cell RNA-sequencing data from the Heart Cell Atlas (Source: https://www.heartcellatlas.org/)[26], which comprises data of heart tissue samples obtained from transplant donors without a history of cardiac disease or arrhythmia. We found that *PKN1 and PKN2* were expressed in cardiac fibroblasts and other cardiac cells (Fig. 1a, b); however, *PKN3* was expressed only in cardiac endothelial cells (Fig. 1c). We performed a quantitative real-time polymerase chain reaction (PCR) analysis to investigate the expression of PKN isoforms in cardiac fibroblasts isolated from adult C57BL6 mice. The PCR analysis revealed that *Pkn1* and *Pkn2* were expressed in adult murine cardiac fibroblasts, with only low expression of *Pkn3* (Fig. 1d). Phosphorylation of PKN1 and PKN2 results in catalytic activation[27,28]. Hence, we investigated whether PKN1 and PKN2 were activated in isolated murine cardiac fibroblasts. Treatment with angiotensin II (AngII) and TGF-β induced PKN1 and PKN2 phosphorylation, suggesting that PKNs were activated in cardiac fibroblasts (Fig. 1e–g).

### Fibroblasts in PKN1/2 deficient mice

To examine the role of PKN1 and PKN2 in fibroblasts in vivo, we generated tamoxifen-inducible fibroblast-specific PKN1/2 double-knockout (Pdgfra-PKN1/2 KO) by mating Pdgfra-Cre-ERT mice with $Pkn1^{flox/flox}$ and $Pkn2^{flox/flox}$ animals[23,29]. To induce Cre-mediated recombination of floxed PKN1/2 alleles, animals were treated with intraperitoneal injections of tamoxifen (1 mg) for 5 consecutive days at the age of 8 weeks, and the efficiency of recombination was determined 10 days later using Western blot analysis (Fig. 2a). PKN1 and PKN2 expressions were strongly reduced in cardiac fibroblasts isolated from

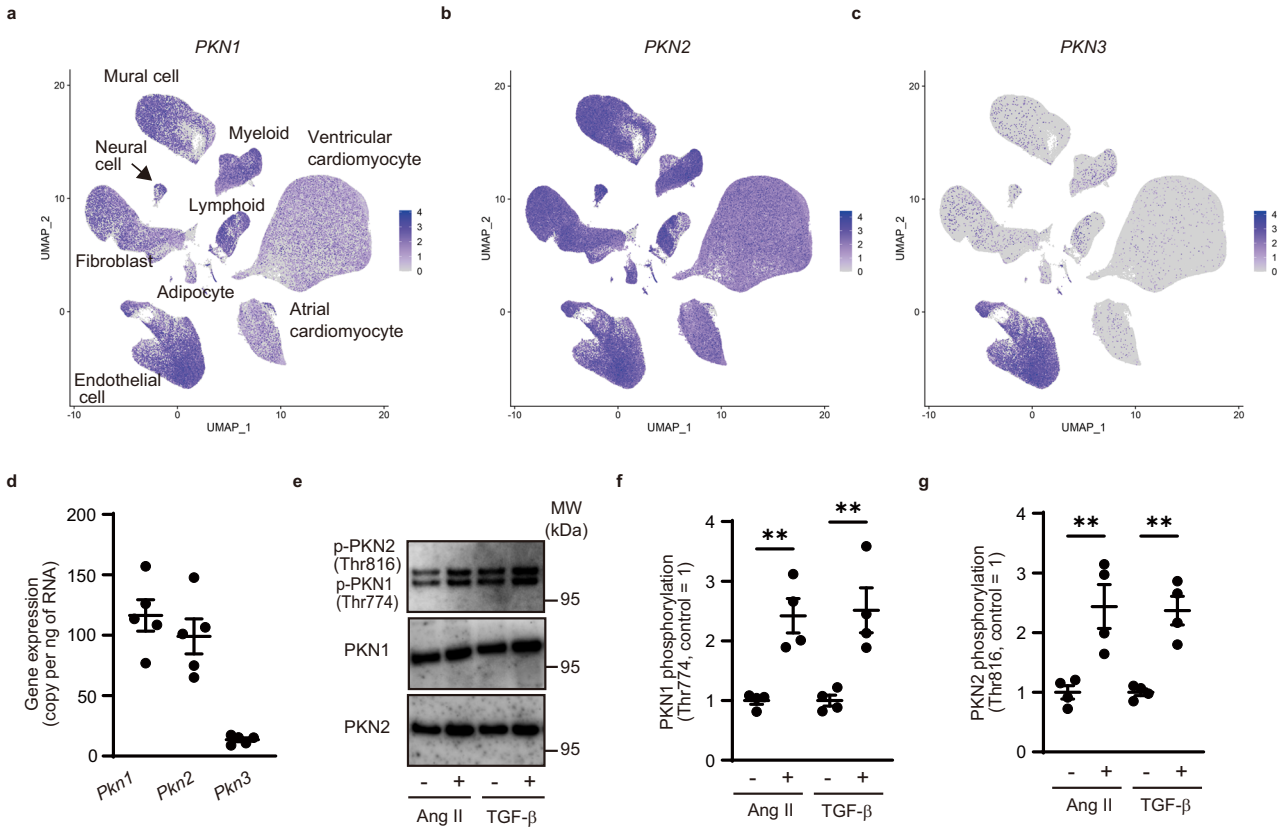


**Fig. 1 | Protein kinase N (PKN) 1 and PKN2 are expressed in cardiac fibroblasts.** **a**–**c** Feature plot of cardiac cells labeled according to *PKN1*, *PKN2*, and *PKN3* transcription expression, visualized using Uniform Manifold Approximation and Projection (UMAP). **d** Quantitative real-time polymerase chain reaction analysis of *Pkn1*, *Pkn2*, and *Pkn3* expression in isolated cardiac fibroblasts ($n = 5$, biological replicates per group). **e** Western blot analysis for PKN1 (Thr774) and PKN2 (Thr816) phosphorylation in cardiac fibroblasts after treatment with angiotensin II (AngII, 100 nM) or TGF-β (10 ng/mL). **f** Statistical evaluation of (**e**) ($n = 4$, biological replicates per group; AngII, $^{**}p = 0.0029$, TGF-β, $^{**}p = 0.0079$). **g** Statistical evaluation of (**e**) ($n = 4$, biological replicates per group; AngII, $^{**}p = 0.0096$, TGF-β, $^{**}p = 0.0014$). Data are presented as the mean ± SEM and analyzed using a two-sided unpaired Student *t* test (**f**, **g**). The data represent three independent experiments with similar results. Source data are provided as a Source Data file.

https://doi.org/10.1038/s41467-024-52068-0

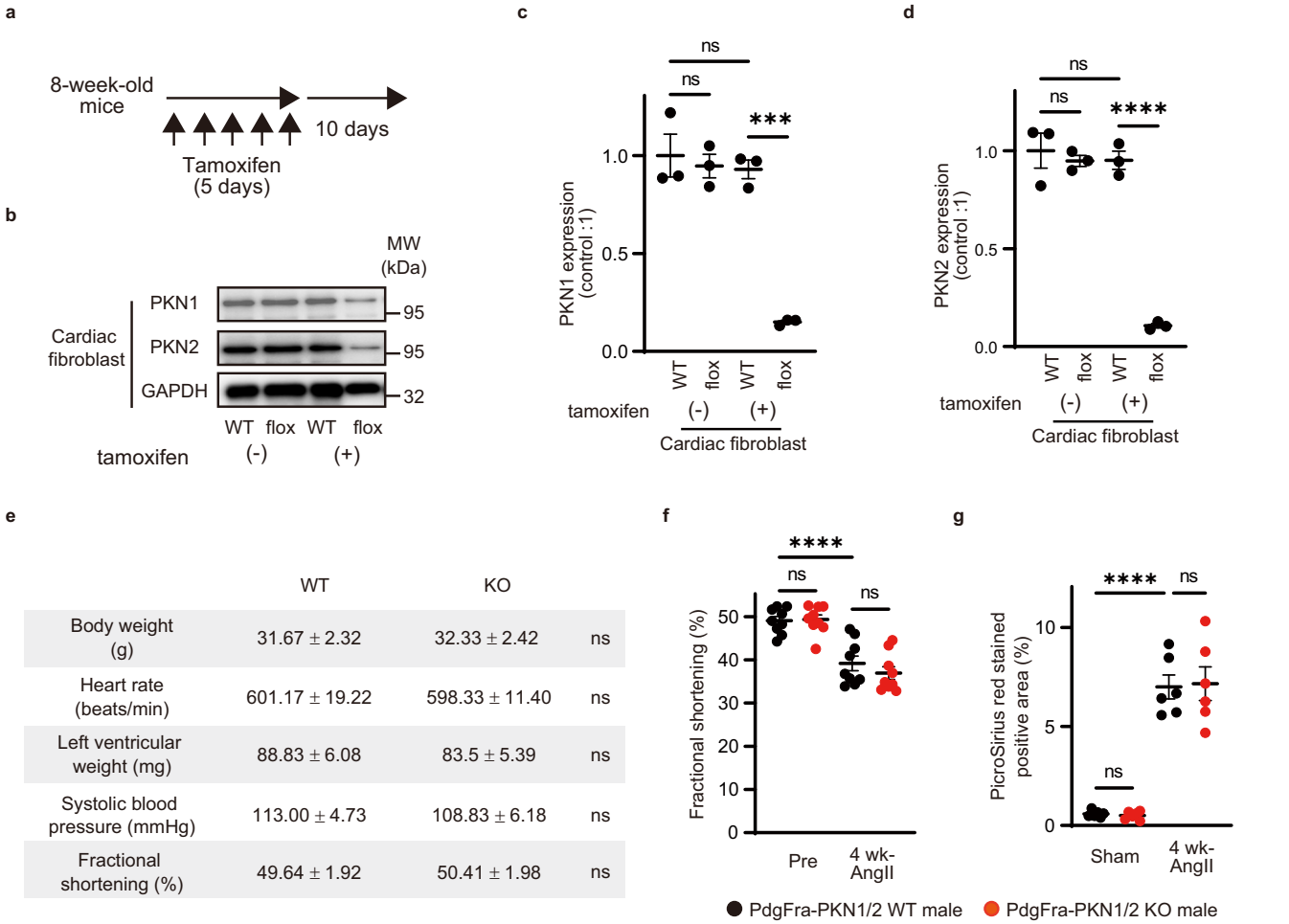


| | WT | KO | |
|---|---|---|---|
| Body weight (g) | 31.67 ± 2.32 | 32.33 ± 2.42 | ns |
| Heart rate (beats/min) | 601.17 ± 19.22 | 598.33 ± 11.40 | ns |
| Left ventricular weight (mg) | 88.83 ± 6.08 | 83.5 ± 5.39 | ns |
| Systolic blood pressure (mmHg) | 113.00 ± 4.73 | 108.83 ± 6.18 | ns |
| Fractional shortening (%) | 49.64 ± 1.92 | 50.41 ± 1.98 | ns |

**Fig. 2 | Fibroblasts in PKN1/2-deficient mice. a** Animals were treated with intraperitoneal injections of tamoxifen for 5 consecutive days, and the efficiency of recombination was determined 10 days later. **b** Western blot analysis for PKN1 and PKN2 in cardiac fibroblasts isolated from the heart of Pdgfra-PKN1/2 WT or KO mice after tamoxifen induction. GAPDH is used for control. **c**, **d** Statistical evaluation of (**b**) ($n = 3$, biological replicates per group). ns, not significant; $^{***}p = 0.0002$; $^{****}p < 0.0001$. **e** Physiological function in Pdgfra-PKN1/2 WT or KO male mice ($n = 6$, biological replicates per group). ns, not significant. **f** Left ventricular fractional shortening assessed using echocardiography ($n = 8$, biological replicates per group) and (**g**) fibrotic changes in left ventricles assessed using Picrosirius red staining ($n = 6$, biological replicates per group) after 4 weeks of sustained AngII infusion (100 ng·g$^{-1}$·d$^{-1}$) in Pdgfra-PKN1/2 WT or KO male mice. ns, not significant; $^{****}p < 0.0001$. Data are presented as the mean ± SEM and analyzed using a two-sided unpaired Student *t* test (**e**) and two-way ANOVA followed by Tukey's post hoc test (**c**, **d**, **f**, **g**). The data represent three independent experiments with similar results. Source data are provided as a Source Data file.

tamoxifen-treated Pdgfra-PKN1/2 KO mice (Fig. 2b–d). PKN1/2 expression in cardiomyocytes was not affected in Pdgfra-PKN1/2 KO mice (Supplementary Fig. 1). No difference in basal cardiac function was observed between Pdgfra-PKN1/2 WT and KO mice (Fig. 2e).

In our model of heart failure, although PKN1/2 in cardiac fibroblasts was phosphorylated by the AngII treatment in vitro (Fig. 1), no differences were observed in AngII-induced cardiac systolic dysfunction and cardiac fibrosis between Pdgfra-PKN1/2 WT and KO mice (Fig. 2f, g). These data suggest that PKN1/2 is expressed in cardiac fibroblasts, and PKN1/2 deletion does not affect basal cardiac function and AngII-induced cardiac dysfunction.

## PKN1/2 deficiency decreased infarct area in MI

TGF-β has been implicated in the pathogenesis of cardiac fibrosis after MI[30]. To examine whether PKN1/2 could mediate MI-induced cardiac fibrosis in vivo, we used an MI with the ischemia-reperfusion (IR) model, where the left anterior descending artery was occluded for 45 min. We examined infarct changes in Picrosirius red-stained sections 7 days after the surgery (Fig. 3a, b). PKN1/2 deficiency decreased cardiac fibrosis in the heart. Next, cardiac functionality was assessed using echocardiography (Fig. 3c), revealing that PKN1/2 deficiency in cardiac fibroblasts protected mice from cardiac left ventricular dilation (Fig. 3d) and systolic dysfunction induced by MI accompanied by IR (Fig. 3e). Moreover, we examined cardiac fibrosis and cardiac function at 28 days postoperatively. PKN1/2 deficiency decreased cardiac fibrosis (Fig. 3f) and protected mice from cardiac left ventricular dilation (Fig. 3g) and systolic dysfunction (Fig. 3h). Although continuous activation of fibroblast and myofibroblast causes heart failure, fibroblast-mediated reparative scarring after MI is critical for maintaining the structural integrity of the ventricular wall to prevent ventricular wall rupture[9]. To investigate whether PKN1/2 deficiency could affect cardiac rupture after MI, we used an MI model of Pdgfra-PKN1/2 WT and KO mice, whose left coronary artery was permanently ligated. Necropsy indicated no difference between Pdgfra-PKN1/2 WT and KO mice when MI-related death occurred, which was accompanied by a blood clot within the chest cavity that resulted from cardiac rupture (Fig. 3i). PKN1/2 deficiency in cardiac fibroblasts protected mice from cardiac systolic dysfunction induced by MI when the left coronary artery was permanently ligated (Fig. 3j). These data suggest that PKN1/2 deficiency in cardiac fibroblast protects mice from cardiac dysfunction induced by both MI model with IR and permanent coronary artery ligation.

https://doi.org/10.1038/s41467-024-52068-0

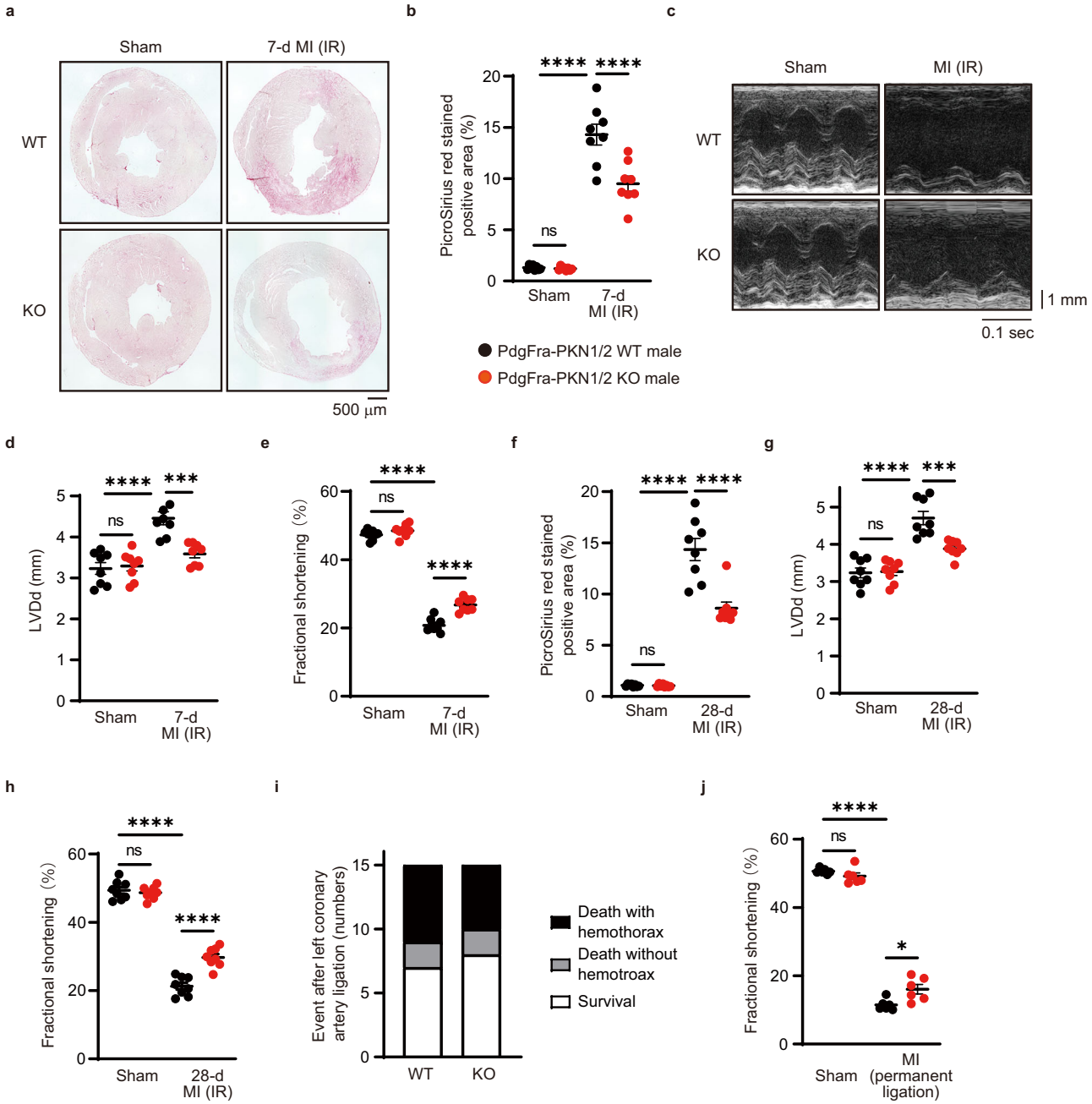


**Fig. 3 | PKN1 and PKN2 deletion in cardiac fibroblasts suppresses cardiac fibrosis after myocardial infarction. a**, **b** Fibrotic changes in the left ventricles after 7 days of myocardial infarction (MI) with the ischemia-reperfusion (IR) model were assessed using Picrosirius red staining ($n = 8$, biological replicates per group). ns, not significant; ****$p < 0.0001$. **c**–**e** Echocardiogram analysis of left ventricular end-diastolic diameter (**d**; LVDd) and fractional shortening (**e**) was performed before and 7 days after MI accompanied by IR ($n = 8$, biological replicates per group). ns, not significant; ***$p = 0.0004$; ****$p < 0.0001$. Fibrotic changes in the left ventricles (**f**), LVDd (**g**), and fractional shortening (**h**) were examined after 28 days of MI with the IR model. ns, not significant; ***$p = 0.0005$; ****$p < 0.0001$. **i** Number of events during 7 days of MI accompanied by permanent ligation of the left coronary artery ($n = 15$, biological replicates per group). **j** Fractional shortening 7 days after permanent ligation of the left coronary artery ($n = 6$, biological replicates per group). ns, not significant; *$p = 0.0108$; ****$p < 0.0001$. Data are presented as the mean ± SEM and analyzed using the two-way ANOVA followed by Tukey's post hoc test (**b**, **d**–**h**, **j**). The data represent three independent experiments with similar results. Source data are provided as a Source Data file.

## PKN1/2 mediated TGF-β induced synthesis of collagen in cardiac fibroblasts

We examined the functional role of PKN1/2 in cardiac fibroblasts using an siRNA-mediated PKN1/2 knockdown (Fig. 4a, b). TGF-β exerts a wide range of actions on fibroblasts, modulating proliferation and migration[31]. TGF-β-treated murine cardiac fibroblasts were stained with antibodies against αSMA and Ki67, a cellular marker for proliferation. Dual immunostaining of αSMA and Ki67 showed no difference in cell proliferation between siControl and siPKN1/2 treatment (Fig. 4c). The results of the scratch wound healing assay to examine the role of PKN1/2 in fibroblast migration are shown in Fig. 4d. The scratch wound closure rate of TGF-β-treated fibroblasts was unaffected by PKN1/2 deletion (Fig. 4e).

Fibroblasts are the primary regulator of cardiac ECM[17]. To investigate whether PKN could regulate collagen synthesis in

https://doi.org/10.1038/s41467-024-52068-0

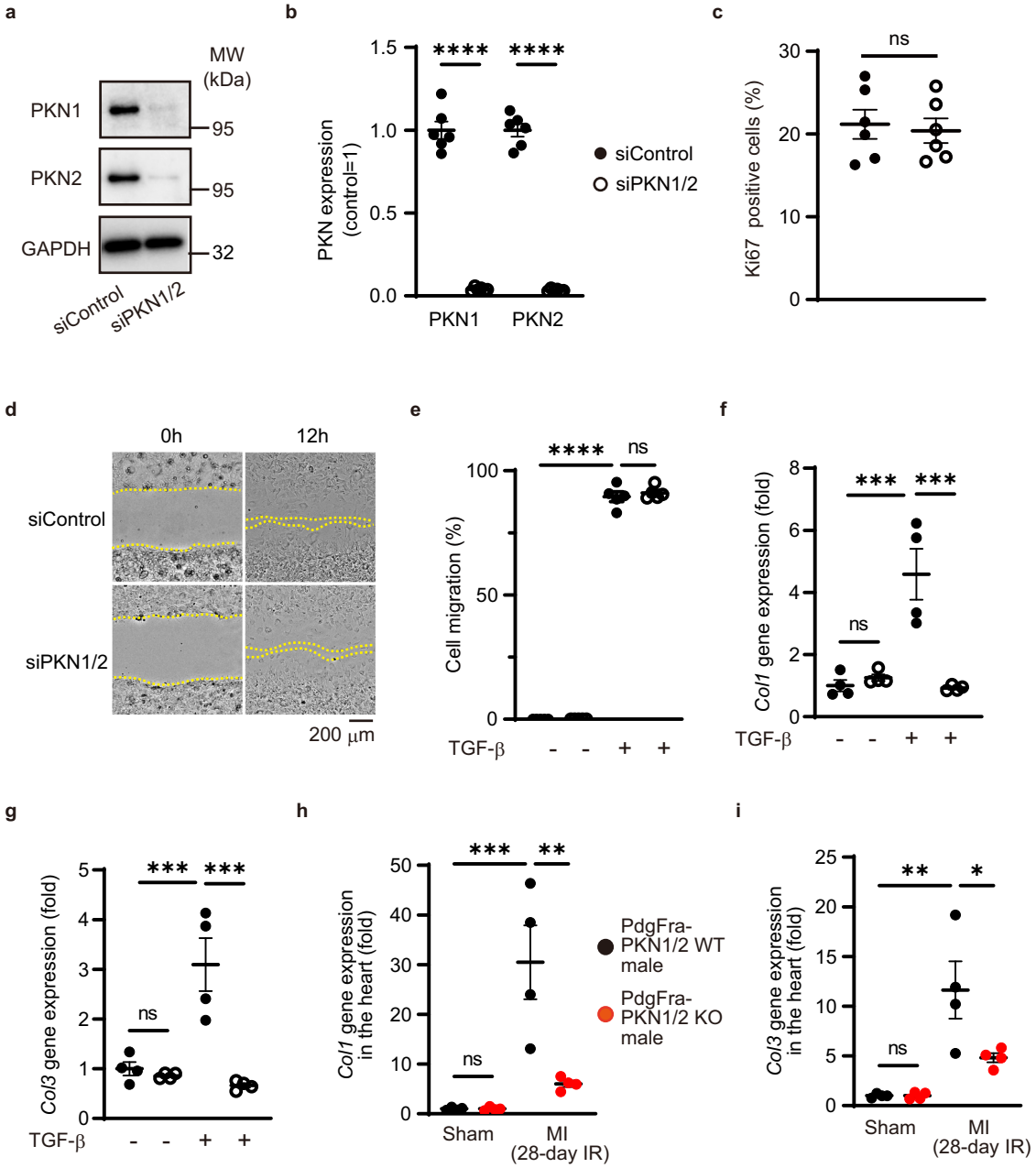


**Fig. 4 | PKN1 and PKN2 deletion in cardiac fibroblasts suppresses the synthesis of collagen. a** Efficiency of PKN1 and PKN2 knockdown in cardiac fibroblasts as shown via western blot analysis. **b** Statistical evaluation of (**a**) ($n = 6$, biological replicates per group). ****$p < 0.0001$. **c** Quantification of the percentage of Ki67-positive cells in αSMA-positive cells ($n = 6$, biological replicates per group). ns, not significant. Scratch wound healing assay (**d**) and quantification (**e**) after 12 h ($n = 5$, biological replicates per group). ns, not significant; ****$p < 0.0001$. **f**, **g** Gene expression of collagen isoforms 1 and 3 (determined by quantitative real-time polymerase chain reaction; $n = 4$, biological replicates per group) after 48 h of TGF-β treatment. ns, not significant; ***$p = 0.0003$ (**f**). ns, not significant; ***$p = 0.0008$ (siControl, TGF-β − vs. siControl, TGF-β +); ***$p = 0.0002$ (siControl, TGF-β + vs. siPKN1/2, TGF-β +) (**g**). **h**, **i** Gene expression of collagen isoforms 1 and 3 (determined by quantitative real-time polymerase chain reaction; $n = 6$, biological replicates per group) in the infarct area after 28 days of an MI with the ischemia-reperfusion (IR) model. ns, not significant; **$p = 0.0028$; ***$p = 0.0006$ (**h**). ns, not significant; *$p = 0.0284$; **$p = 0.0012$ (**i**). Data are presented as the mean ± SEM and analyzed using a two-sided unpaired Student *t* test (**b**, **c**) and *t*wo-way ANOVA followed by the Tukey's post hoc test (**e**, **f**, **g**, **h**, **i**). The data represent three independent experiments with similar results. Source data are provided as a Source Data file.

cardiac fibroblasts, the expression of collagen isoforms was examined using quantitative real-time PCR. The treatment with siPKN1/2 reduced TGF-β-induced collagen expression in vitro (Fig. 4f, g). Moreover, quantitative real-time PCR showed that MI-induced collagen expression in the heart was decreased in Pdgfra-PKN1/2 KO mice (Fig. 4h, i). These data suggest that PKN1/2 in cardiac fibroblasts mediates cardiac fibrosis through collagen synthesis and not through their proliferation and migration.

## PKN1/2 deficiency decreased MI-induced conversion of fibroblast into myofibroblast

Cardiac fibroblast activation plays a central role in MI, as the sudden death of many cardiomyocytes stimulates inflammation and subsequent activation of myofibroblasts, leading to scar formation[32]. TGF-β-mediated cell state transitions of cardiac fibroblasts to a myofibroblast phenotype accelerates fibrotic matrix deposition[17]. To investigate whether PKN1/2 is involved in TGF-β-induced conversion of fibroblasts

into myofibroblasts, we performed an immunostaining analysis in isolated murine cardiac fibroblasts 48 h after TGF-β stimulation (Fig. 5a). TGF-β stimulation decreased the number of fibroblasts expressing PDGFRα, a mesenchymal marker for cardiac fibroblasts (Fig. 5b)[33], and increased the formation of αSMA-positive stress fibers (Fig. 5c). PKN1/2 deletion suppressed TGF-β-induced conversion of fibroblasts into myofibroblasts.

We investigated whether PKN1/2 could mediate the conversion of fibroblasts into myofibroblasts in the MI with IR model in vivo. In Pdgfra-PKN1/2 WT mice, MI accompanied by IR increased the intensity of αSMA and vimentin, a fibroblast and myofibroblast marker[34], in the infarct area at 7 days after the 45-min reperfusion (Fig. 5d). No differences were observed in the number of vimentin-positive cells in the infarct area between Pdgfra-PKN1/2 WT and KO mice (Fig. 5e). PKN1/2 deficiency decreased MI accompanied by IR-induced increase in vimentin and αSMA double-positive cells (Fig. 5f). Moreover, we examined vimentin- and αSMA-positive cells at 28 days post-operatively. PKN1/2 deficiency decreased the IR-induced increase of vimentin and αSMA double-positive cells (Fig. 5g, h). These data suggest that PKN1/2 accelerates the conversion of fibroblasts into myofibroblasts in the infarct area.

### PKN1/2 activated Smad-independent pathways in cardiac fibroblasts

TGF-β regulates the conversion of fibroblasts into myofibroblasts through Smad-dependent and -independent pathways[35]. To investigate whether TGF-β could activate Smad and non-Smad cascades, we examined the phosphorylation of endogenous Smad2, p38, and MRTFA in cardiac fibroblasts isolated from murine hearts. Immunoblotting analysis showed that TGF-β activation increased the phosphorylation of Smad2 (Ser465/467) and p38 (Thr180/182) but not of MRTFA (Thr57) (Fig. 6a and Supplementary Fig. 2). PKN1/2 knockdown significantly reduced TGF-β-mediated p38 phosphorylation, but not that of Smad2 (Fig. 6b–d).

Moreover, we examined the phosphorylation of endogenous Smad3(Ser423/425) in cardiac fibroblasts. Immunostaining assay showed that TGF-β activation increased the Smad3 phosphorylation and that PKN1/2 knockdown did not affect TGF-β-mediated Smad3 phosphorylation (Fig. 6e, f). Subsequently, we examined p38 phosphorylation via an immunostaining assay (Fig. 6g). TGF-β increased the number of cardiac fibroblasts stained with phosphorylated p38. However, PKN1/2 knockdown significantly decreased the TGF-β-induced increase in fibroblasts stained with phosphorylated p38 (Fig. 6h).

To investigate whether PKN1/2 is involved in TGF-β-induced conversion of fibroblasts into myofibroblasts through p38 activation, GFP-tagged PKN catalytic domain (PKN-cat) was overexpressed in isolated murine cardiac fibroblasts (Fig. 7a). Immunostaining analysis showed that GFP-tagged PKN-cat increased the number αSMA-positive fibroblasts and that treatment with p38 inhibitor decreased the number of αSMA-expressing fibroblasts (Fig. 7b, c). The p38 mitogen-activated protein kinase (MAPK) cascades are major signaling pathways that regulate physiological and pathological functions, and MKK3/6 is mainly involved in p38 activation[36]. MKK3/6 is activated by its phosphorylation in the activation loop. We examined whether PKN1/2 could activate MKK3/6 phosphorylation in cardiac fibroblasts (Fig. 7d). The immunostaining assay showed that TGF-β increased the number of cardiac fibroblasts stained with phosphorylated MKK3/6; however, PKN1/2 knockdown significantly decreased the TGF-β-induced increase in fibroblasts stained with phosphorylated MKK3/6 (Fig. 7e). Finally, we examined whether PKN1/2 could mediate MAPK cascades in vivo. Phosphorylation of p38 was increased in the border area's fibroblasts in the MI accompanied by 3-d and 28-d IR model, and Pdgfra-PKN1/2 KO decreased p38 phosphorylation (Fig. 7f, g). These data indicate that PKN1/2 contributes to TGF-β-mediated p38 activation, a Smad-independent pathway, in cardiac fibroblasts in vitro and in vivo.

### PKN1/2 deletion in cardiac fibroblasts prevented cardiac diastolic dysfunction in HFpEF

In vitro, TGF-β stimulation increases gene expression of αSMA in primary cardiac fibroblast in patients with HFpEF[37]. To examine the pathological role of PKN1/2 in other heart failure models in vivo, we used a two-hit pre-clinical mouse model that resembles human HFpEF[38]. In Pdgfra-PKN1/2 WT and KO male mice, obesity and a metabolic syndrome were induced by feeding mice a high-fat diet (HFD), and hypertension was induced by treatment with L-NAME (nitric oxide synthase inhibitor). Cardiomyocyte-specific PKN1/2 deficient male mice (cmc-PKN1/2 KO) were also exposed to this combination of HFD and L-NAME because PKN1 and PKN2 are expressed in cardiomyocytes[23]. The 10-week combination of HFD and L-NAME equally increased body weight and systolic blood pressure in Pdgfra-PKN1/2 WT and KO mice, as well as in cmc-PKN1/2 WT and KO male mice (Table 1). The combination of HFD and L-NAME resulted in typical clinical HFpEF features, including cardiac hypertrophy[38]. HFD/L-NAME-induced cardiac hypertrophy was unaffected in Pdgfra-PKN1/2 WT and KO mice, as well as in cmc-PKN1/2 KO WT and KO male mice. Cardiac fibrosis was also evaluated after the 10-week HFD and L-NAME exposure, using Picrosirius red staining. The cardiac fibrotic area induced by the combination treatment was significantly reduced in Pdgfra-PKN1/2 KO mice, but not in cmc-PKN1/2 KO mice (Fig. 8a, b). Next, echocardiography was performed before and after the 5- and 10-week HFD feeding and L-NAME exposure. In Pdgfra-PKN1/2 WT and KO male mice, no difference was observed in fractional shortening, suggesting comparable systolic function (Fig. 8c). PKN1/2 deficiency in cardiomyocytes did not affect cardiac systolic function (Fig. 8d).

We measured early diastolic mitral inflow velocity (E) and annular velocity (E') and calculated the ratio of E to E' (E/E') (Fig. 8e), predictive of left ventricular filling pressures and increases in the presence of left ventricular diastolic dysfunction[39]. The combination of HFD and L-NAME resulted in increased E/E'. Of note, Pdgfra-PKN1/2 KO mice were resistant to HFD- and L-NAME-induced increase in E/E' (Fig. 8f), but cmc-PKN1/2 mice were not (Fig. 8g). Hemodynamic measurements via cardiac catheterization, the standard for assessing diastolic function, were performed (Fig. 8h)[40]. In Pdgfra-PKN1/2 WT male mice, the 10-week combination of HFD and L-NAME resulted in an increased end-diastolic pressure-volume relationship (EDPVR), a defining feature of diastolic dysfunction. Pdgfra-PKN1/2 KO suppressed the increased EDPVR. Sex is known to influence cardiovascular disease, with women being predisposed to HFpEF[41]. The HFD- and L-NAME-induced increase in E/E' was suppressed in Pdgfra-PKN1/2 KO female mice (Fig. 8i and Supplementary Fig. 3). These data suggest that PKN1/2 in fibroblasts, but not in cardiomyocytes, mediates HFD and L-NAME-induced cardiac diastolic dysfunction both in male and female mice.

### PKN1/2 contributed to fibroblast conversion into myofibroblast in HFpEF

We investigated whether PKN1/2 could mediate the conversion of fibroblasts into myofibroblasts in vivo in the heart using the HFD/L-NAME-induced HFpEF model. In Pdgfra-PKN1/2 WT mice, the intensity of αSMA was increased in vimentin-positive cells after the 10-week HFD and L-NAME exposure (Fig. 9a). PKN1/2 deficiency decreased HFD/L-NAME-induced increase in vimentin and αSMA double-positive cells (Fig. 9b). To investigate whether the combination of HFD and L-NAME activates Smad and non-Smad cascades, we examined Smad3 and p38 phosphorylation via an immunostaining assay. No differences were observed in the number of Pdgfra- and phospho-Smad3-positive cells in the heart between

https://doi.org/10.1038/s41467-024-52068-0

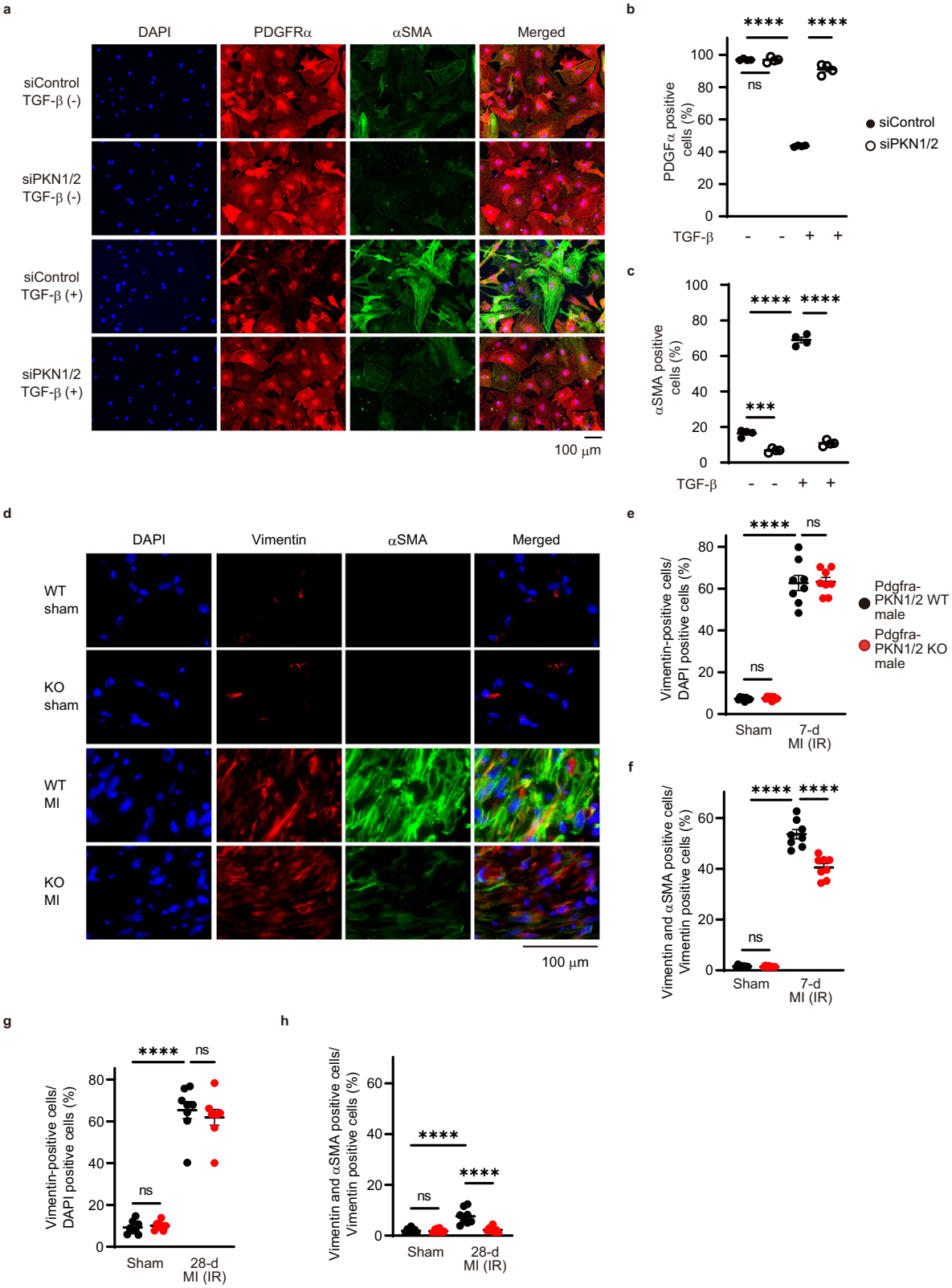


Pdgfra-PKN1/2 WT and KO mice (Fig. 9c). The combination of HFD and L-NAME increased p38 phosphorylation in Pdgfra-positive cells in the heart; however, Pdgfra-PKN1/2 KO significantly decreased the HFD/L-NAME-induced p38 phosphorylation in fibroblasts (Fig. 9d, e). These data suggest that PKN1/2 contributes to the conversion of fibroblasts into myofibroblasts through p38 activation in HFD and L-NAME-induced heart failure.

## Discussion

Owing to the dysregulation of protein kinase activity in many diseases, the protein kinase family has become one of the most important drug targets in the last decade[42]. We recently have demonstrated that cardiomyocyte-specific PKN1/2 deficiency decreases AngII- or pressure overload-induced cardiac hypertrophy in vivo[23]. Beyond the cardiomyocyte-centric view of heart failure, it is now accepted that

**Fig. 5 | PKN1 and PKN2 deletion suppresses the differentiation of cardiac fibroblasts after MI. a** Immunofluorescent images of siRNA-treated cardiac fibroblasts immunostained for α-smooth muscle actin (αSMA)-positive stress fibers (green), PDGFRα (red), and nuclei (blue). Quantification of PDGFRα-positive cells (**b**) and αSMA-positive cells (**c**) shown as a percentage of DAPI-positive cells ($n = 4$, biological replicates per group). ns, not significant; ***$p = 0.0001$; ****$p < 0.0001$. **d** Immunofluorescent staining of fibroblasts and myofibroblasts in the cardiac infarction area 7 days after injury. The fibroblasts and myofibroblasts were immunostained for vimentin (red), αSMA (green), and nuclei (blue). **e** Quantification of vimentin-positive cells shown as a percentage of DAPI-positive cells ($n = 6$, biological replicates per group). ns, not significant; ****$p < 0.0001$. **f** Quantification of dual-positive cells for vimentin and αSMA shown as a percentage of vimentin-positive cells ($n = 6$, biological replicates per group). ns, not significant; ****$p < 0.0001$. **g** Quantification of vimentin-positive cells in the cardiac infarction area 28 days after injury ($n = 8$, biological replicates per group). ns, not significant; ****$p < 0.0001$. **h** Quantification of dual-positive cells for vimentin and αSMA shown as a percentage of vimentin-positive cells 28 days after injury ($n = 8$, biological replicates per group). ns, not significant; ****$p < 0.0001$. Data are presented as the mean ± SEM and analyzed using two-way ANOVA followed by Tukey's post hoc test (**b**, **c**, **e**, **f**, **g**, **h**). The data represent three independent experiments with similar results. Source data are provided as a Source Data file.

alterations in the interstitial ECM also play a major role in the development of pathological structural remodeling of the myocardium that determines the evolution of heart failure[7]. The current study examined whether PKN1/2 could be a potential therapeutic target for heart failure after coronary artery reperfusion, given that the development of heart failure following MI accompanied by IR is closely associated with cardiac fibrosis (i.e., profound alterations in cardiac geometry, function, and structure). Although the extent of fibrotic remodeling is closely associated with heart failure, myocardial fibrosis is not necessarily the primary cause of dysfunction[43]. In the acute phase of MI, the loss of a significant number of cardiomyocytes triggers a reparative sequence, leading to fibrous tissue formation[43]. The fibrous scar is critical to protect the heart from rupture by preserving the structural integrity of the ventricle.

We observed no difference in cardiac rupture events after MI between PKN1/2 WT mice and KO mice. A lineage-tracing reporter system has shown that cardiac-activated fibroblasts and myofibroblasts proliferate in the border zone, and they robustly move into the infarct area within 2 days after MI injury[44]. In vitro, fibroblasts with PKN1/2 deletion continue to exhibit cell proliferation and migration, which may protect the heart from rupture. ECM deposition in the heart initially represents an adaptive response to increase structural integrity and prevent cardiac rupture in MI; however, extensive and sustained fibrosis impairs heart function[13]. Fibroblasts are converted to myofibroblasts, and activated cardiac fibroblasts are the primary source of ECM molecules such as collagens and fibronectin[30]. We found that PKN1/2 deletion suppresses the differentiation of fibroblasts into myofibroblasts in vitro and in vivo and decreases collagen I and III expression after MI, suggesting that the PKN1/2 present in cardiac fibroblasts mediates ECM production after MI through fibroblast differentiation without affecting migration and proliferation rates.

HFpEF currently accounts for >50% of all heart failure cases, and large trials testing neurohumoral inhibition in HFpEF failed to reach a positive outcome[45]. Left ventricular diastolic dysfunction is a key defining feature of HFpEF[46]. The heart comprises a myocytic compartment and a non-myocytic compartment, and both compartments contribute to diastolic stiffness[47]. In this study, cardiomyocyte-specific PKN1/2 deficiency did not affect cardiac stiffness. In addition to systolic dysfunction, cardiac fibrosis is associated with diastolic dysfunction[11]. Pathophysiologic stimuli, such as metabolic dysfunction and aging, may cause interstitial fibrosis in the absence of infarction[43]. We found that PKN1/2 deficiency in fibroblasts decreased the cardiac fibrosis in HFpEF induced by the combination of HFD and L-NAME, resulting in improved cardiac diastolic function. These data suggest that PKN1/2 plays a more crucial role in fibroblasts than in cardiomyocytes in HFpEF.

There are marked sex differences in cardiovascular diseases, with HFpEF being more prevalent in women. In the current study, fibroblast-specific PKN1/2 deficiency started to improve cardiac diastolic function at 5 weeks after the start of combination exposure to HFD and L-NAME in male mice, but this was only observed after 10 weeks in female mice. PKN1/2 deficiency attenuated HFD- and L-NAME-induced cardiac diastolic dysfunction earlier in males than in females. In HFD- and L-NAME-induced HFpEF models, female mice develop a more significantly attenuated cardiac phenotype than their male counterparts[48], which may explain the sex differences in the current study. Further research is warranted to confirm the role of PKN1/2 in sex differences.

We recently have shown that AngII increases PKN-mediated MRTFA phosphorylation in cardiomyocytes[23]. In the present study, PKN1/2 deficiency in fibroblasts did not affect AngII-induced cardiac fibrosis. No difference was observed in MRTFA phosphorylation between cardiac fibroblasts with and without TGF-β treatment. This suggests that the cell type-specific phosphorylation signaling mediated by PKN1/2 contributes to various cardiac diseases.

In cardiac fibrosis, TGF-β regulates Smad-dependent signaling and Smad-independent pathways[32]. TGF-β signaling activates Smad complexes, which translocate into the nucleus to regulate transcription of target genes[35]. In vitro, TGF-β activation increases Smad3 phosphorylation in rat cardiac fibroblasts[49]. In the heart, Smad3 activation in fibroblasts is involved in post-MI repair, restraining fibroblast proliferation and contributing to scar organization by stimulating integrin synthesis[50]. The current study found no difference in TGF-β-induced and HFD- and L-NAME-induced Smad phosphorylation between cardiac fibroblasts with and without PKN1/2 deletion. Smad2/3 is activated through their carboxy-terminal phosphorylation, mainly by TGF-β receptor kinases[35]. Collectively, these findings suggest that Smad2/3 is activated without PKN1/2 activation in cardiac fibroblasts.

TGF-β regulates Smad-independent pathways, including the p38 MAPK pathway. The balance between the Smad activation and the p38 MAPK pathway often defines cellular responses to TGF-β. In cardiac fibroblasts, p38 deletion reduces cardiac fibrosis and cardiac diastolic dysfunction, which is induced by MI accompanied by IR[34]. Phosphorylation alters p38 folding and stabilizes the activation loop in an open conformation[51]. Phosphorylated p38 induces a state transition from quiescent fibroblast to myofibroblast to produce ECM. Moreover, MKK3 and MKK6 are mainly involved in p38 activation[36]. Continuous MKK6 activation increases αSMA-positive fibroblasts and tissue fibrosis through p38 activation in various organs, including the heart[34]. We showed that TGF-β stimulation increased p38 and MKK3/6 phosphorylation in cardiac fibroblasts, and PKN1/2 deficiency significantly decreased TGF-β-induced p38 and MKK3/6 phosphorylation in vitro and MI-induced p38 phosphorylation in vivo. This regulation of MAPK cascades is complex as p38 can respond to many stimuli and can be activated through at least a dozen kinases[52]. Although further studies are needed to identify the PKN1/2-phosphorylated molecules, these studies support that PKN1/2-induced phosphorylation of p38 mediates the conversion of cardiac fibroblasts into myofibroblasts (Fig. 9f).

In conclusion, PKN1/2 activation mediates cardiac fibrosis by converting cardiac fibroblasts into myofibroblasts without affecting fibroblast migration or proliferation. Moreover, removing PKN1/2 from fibroblasts prevents cardiac fibrosis in murine models of MI and HFpEF model mice. This indicates that PKN1/2 is a potential treatment target for cardiac fibrosis in heart failure.

https://doi.org/10.1038/s41467-024-52068-0

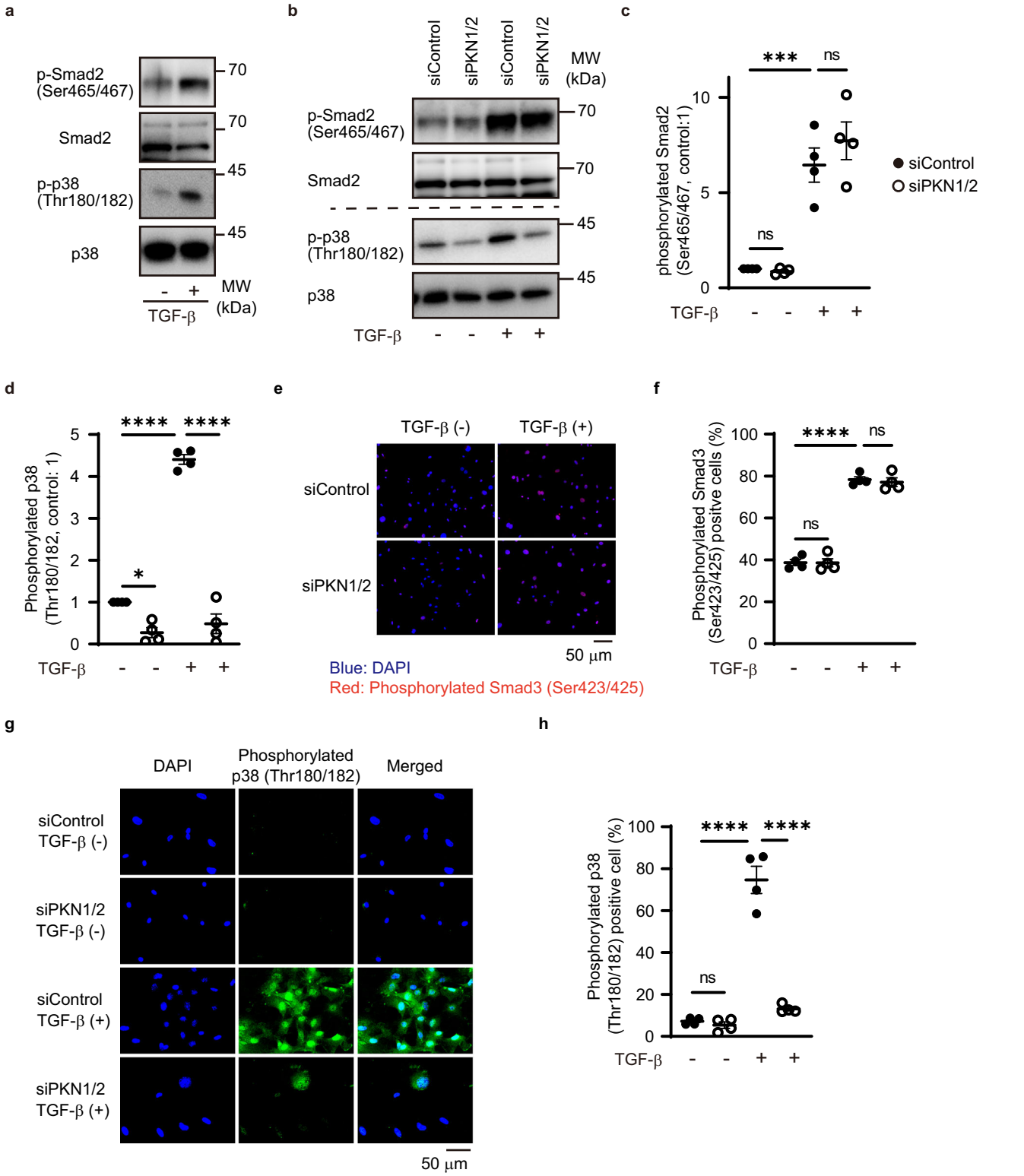


**Fig. 6 | PKN1/2 knockdown significantly reduced TGF-β-mediated p38 phosphorylation. a** Western blot analysis for TGF-β-mediated phosphorylation of Smad2 (Ser465/467) and p38 (Thr180/182) in cardiac fibroblasts. The results represent three independent experiments. Western blot analysis (**b**) and quantification for TGF-β-mediated phosphorylation of endogenous Smad2 (**c**) and p38 (**d**) in cardiac fibroblasts after siRNA-mediated PKN1/2 knockdown ($n = 4$, biological replicates per group). ns, not significant; $^{*}p = 0.0169$; $^{***}p = 0.0005$; $^{****}p < 0.0001$. Immunofluorescent images (**e**) and quantification of the number (**f**) of cardiac fibroblasts with phosphorylated Smad3 (Ser423/425; red) after siRNA-mediated PKN1/2 knockdown and TGF-β treatment ($n = 4$, biological replicates per group). ns, not significant; $^{****}p < 0.0001$. Immunofluorescent images (**g**) and quantification of the number (**h**) of cardiac fibroblasts with phosphorylated p38 (green) after siRNA-mediated PKN1/2 knockdown and TGF-β treatment ($n = 4$, biological replicates per group). ns, not significant; $^{****}p < 0.0001$. Data are presented as the mean ± SEM and analyzed using two-way ANOVA followed by Tukey's post hoc test (**c**, **d**, **f**, **h**). The data represent three independent experiments with similar results. Source data are provided as a Source Data file.

https://doi.org/10.1038/s41467-024-52068-0

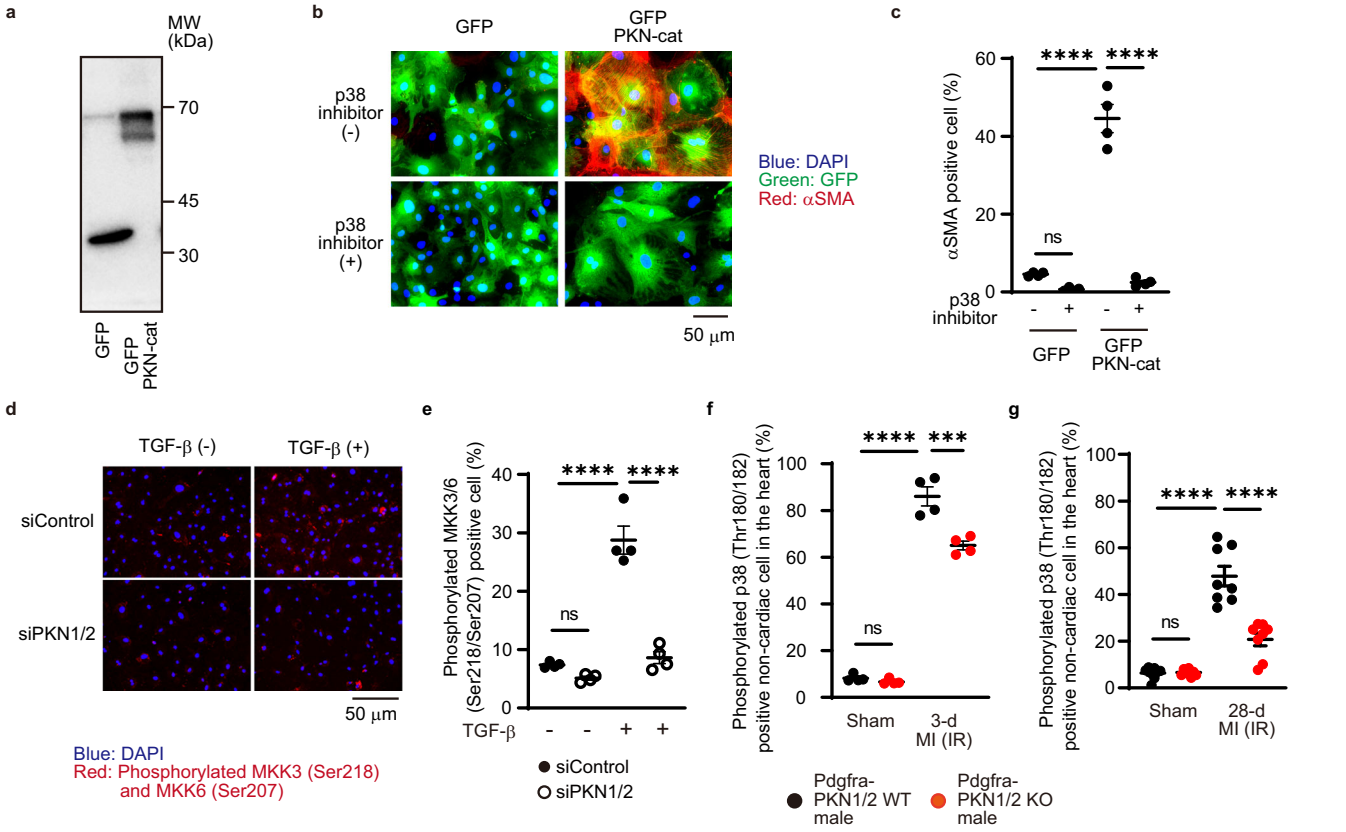


**Fig. 7 | PKN1/2 knockdown significantly reduced MI-induced p38 phosphorylation. a** Western blot analysis for GFP-PKN-cat expression in cardiac fibroblasts. The results represent three independent experiments. Immunofluorescent images (**b**. blue, DAPI; green, GFP; red, αSMA) and quantification of the number (**c**) of αSMA-positive cardiac fibroblasts after overexpression of GFP-PKN-cat and treatment with a p38 inhibitor (10 μM, $n = 4$, biological replicates per group). ns, not significant; $^{****}p < 0.0001$. Immunofluorescent images (**d**) and quantification of the number (**e**) of cardiac fibroblasts with phosphorylated MKK3/6 (Ser218/Ser207, red) and DAPI (blue) after siRNA-mediated PKN1/2 knockdown and TGF-β treatment ($n = 4$, biological replicates per group). ns, not significant; $^{****}p < 0.0001$. Immunofluorescent-based quantification of dual-positive cells for PDGFRα and phosphorylated p38 shown as a percentage of PDGFRα-positive cells in the control and ischemia-reperfusion hearts at 3 days (**f**, $n = 4$, biological replicates per group) and 28 days (**g**, $n = 8$, biological replicates per group) after injury. ns, not significant; $^{***}p = 0.0001$; $^{****}p < 0.0001$. Data are presented as the mean ± SEM and analyzed with two-way ANOVA followed by Tukey's post hoc test (**c**, **e**, **f**, **g**). The data represent three independent experiments with similar results. Source data are provided as a Source Data file.

**Table 1 | Comparison of the effects of the 10-week combination exposure to HFD and L-NAME on Pdgfra-PKN1/2 WT and KO and on cmc-PKN1/2 WT and KO male mice**

| | Control | | HFpEF | | |
|---|---|---|---|---|---|
| | Pdgfra- $PKN^{wt/wt}$ ($n = 10$) | Pdgfra- $PKN^{flox/flox}$ ($n = 10$) | Pdgfra- $PKN^{wt/wt}$ ($n = 10$) | Pdgfra- $PKN^{flox/flox}$ ($n = 10$) | |
| Body weight (g) | 21.15 ± 1.27 | 20.08 ± 0.87 | 38.31 ± 2.45 | 39.37 ± 3.35 | ns |
| Systolic blood pressure (mmHg) | 105.1 ± 10.3 | 106.1 ± 8.2 | 134.4 ± 14.9 | 135.3 ± 9.3 | ns |
| Heart weight/Tibia length (mg/mm) | 5.06 ± 0.10 | 4.90 ± 0.07 | 5.90 ± 0.16 | 5.85 ± 0.12 | ns |
| | cmc-$PKN^{wt/wt}$ ($n = 6$) | cmc-$PKN^{flox/flox}$ ($n = 6$) | cmc-$PKN^{wt/wt}$ ($n = 6$) | cmc-$PKN^{flox/flox}$ ($n = 6$) | |
| Body weight (g) | 26.13 ± 1.17 | 25.72 ± 1.22 | 39.17 ± 2.32 | 39.50 ± 2.17 | ns |
| Systolic blood pressure (mmHg) | 107.3 ± 6.9 | 106.8 ± 3.1 | 138.7 ± 4.6 | 140.5 ± 8.1 | ns |
| Heart weight/Tibia length (mg/mm) | 4.88 ± 0.32 | 4.80 ± 0.28 | 5.96 ± 0.49 | 6.28 ± 0.55 | ns |

Body weight, systolic blood pressure, and ratio of heart weight to tibial length after 10-week combination exposure to HFD and L-NAME in Pdgfra-PKN1/2 WT and KO, and in cmc- PKN1/2 WT and KO male mice. Data are presented as the mean ± SEM and analyzed using two-way ANOVA followed by Tukey's post hoc test. ns, not significant. The data represent three independent experiments with similar results. Source data are provided as a Source Data file.

# Methods

## Study approval

All animal procedures in this study were approved by the Animal Ethics Review Board of the Nagoya University School of Medicine (M240111) and were conducted in accordance with official guidelines and regulations.

## Materials and chemicals

Antibodies to vimentin (1:1000, ab45939), Ki67 (1:1000, ab15580) and phospho-Smad3 (1:100, ab52903) were obtained from Abcam (Cambridge, UK). PKN1 (1:1000, sc-1842) and MRTFA (1:1000, sc-21558) were obtained from Santa Cruz Biotechnology (Dallas, TX, USA). Antibodies to CD45 (1:100, #70257), PKN2 (1:1000, #2612S),

https://doi.org/10.1038/s41467-024-52068-0

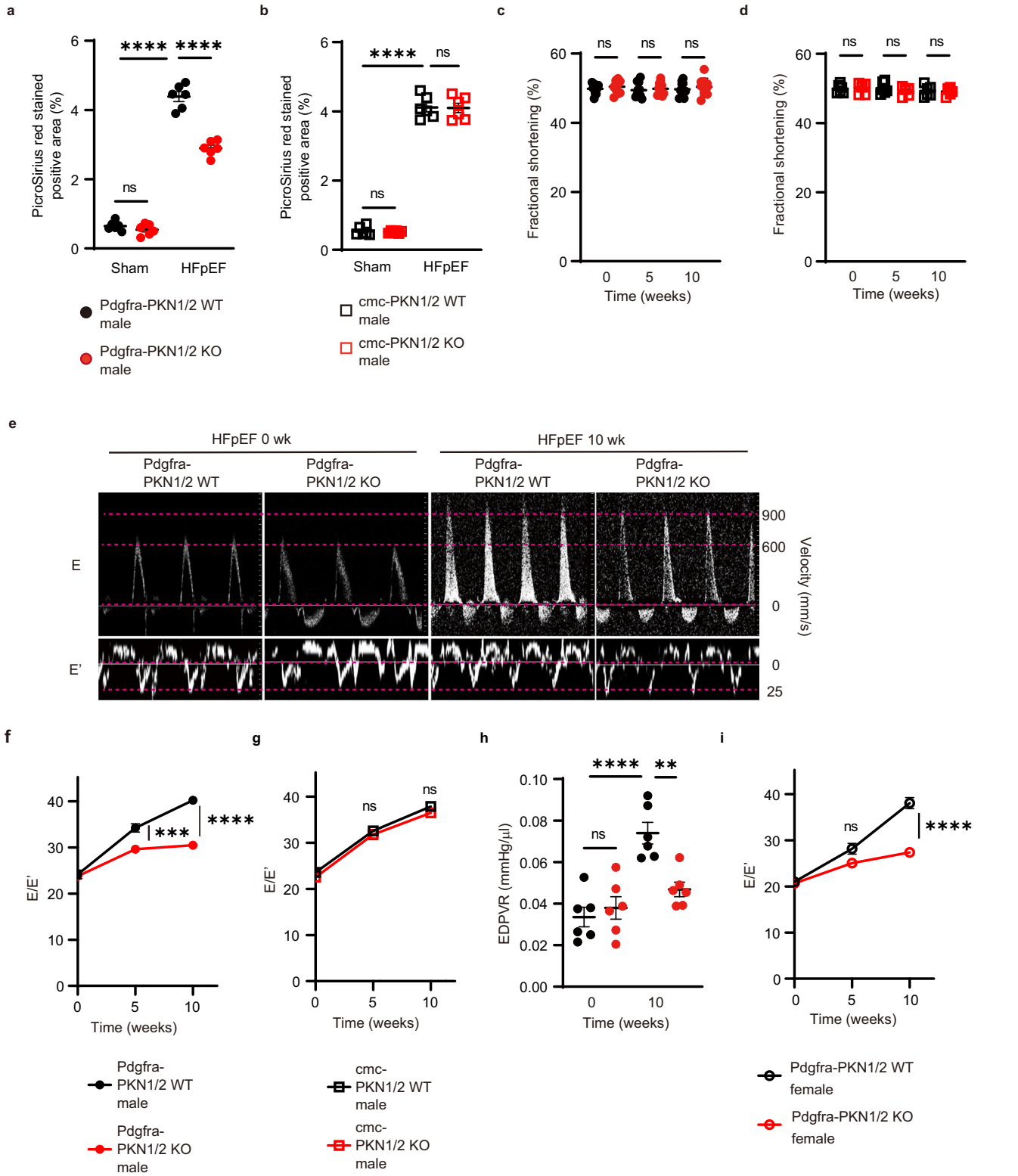


phospho-PKN1/2 (1:1000, #2611S), phospho-p38 MAPK (1:1000, #4511), p38 MAPK (1:1000, #8690), phospho-MKK3/6 (1:1000, #12280), phospho-SMAD2 (1:1000, #18338), and smad2/3 (1:1000, #8685) were obtained from Cell Signaling Technology (Danvers, MA, USA). We used antibodies to CD31 (1:200, #553370, BD Biosciences, San Jose, CA, USA), PDGFRα (1:1000, AF1062, R &D Systems, Minneapolis, MN, USA), αSMA (1:1000, C6198, Sigma-Aldrich, St. Louis, MO, USA), and DAPI (1:1000, D523, Dojindo, Kumamoto, Japan). An antibody to phospho-MRTFA (1:200) was purified as previously described[23].

### PKN gene expression

PKN expression in cardiac cells was analyzed using a publicly available dataset from the Heart Cell Atlas (https://www.heartcellatlas.org/). R (4.1.0, The R Foundation for Statistical Computing, Vienna, Austria) and Seurat (4.3.0, Satija lab, New York, NY, USA) were used for

**Fig. 8 | PKN 1/2 deletion in resident cardiac fibroblasts, not in cardiomyocytes, suppressed cardiac fibrosis in HFpEF.** Fibrotic changes in left ventricles assessed using Picrosirius red staining at 10 weeks after combination exposure to HFD and L-NAME in Pdgfra-PKN1/2 WT and KO mice (**a**) and in cardiomyocyte-specific PKN1/2 (cmc-PKN1/2) WT and KO mice (**b**) ($n = 6$, biological replicates per group). ns, not significant; $^{****}p < 0.0001$. Fraction shortening examined using echocardiography at 0, 5, and 10 weeks after combination exposure to HFD and L-NAME in Pdgfra-PKN1/2 WT and KO mice (**c**) ($n = 10$, biological replicates per group) and in cmc-PKN1/2 WT and KO mice (**d**) ($n = 6$, biological replicates per group). ns, not significant. **e** Representative early diastolic mitral inflow velocity (top) and annular velocity (bottom). Mitral E and E' waves (E/E') ratio at 0, 5, and 10 weeks after combination exposure to HFD and L-NAME in Pdgfra-PKN1/2 WT and KO male mice (**f**) ($n = 10$, biological replicates per group), and in cmc-PKN1/2 mice WT and KO male mice (**g**) ($n = 6$, biological replicates per group). ns, not significant; $^{***}p = 0.0006$; $^{****}p < 0.0001$. **h** End-diastolic pressure-volume relationship (EDPVR) obtained by cardiac catheterization at 0 and 10 weeks after combination exposure to HFD and L-NAME in Pdgfra-PKN1/2 WT and KO mice ($n = 6$, biological replicates per group). ns, not significant; $^{**}p = 0.0035$; $^{****}p < 0.0001$. **i** E/E' at 0, 5, and 10 weeks after combination exposure to HFD and L-NAME in Pdgfra-PKN1/2 WT and KO female mice ($n = 6$, biological replicates per group). ns, not significant; $^{****}p < 0.0001$. Data are presented as the mean ± SEM and analyzed using two-way ANOVA followed by Tukey's post hoc test (**a**–**d**, **h**), or with two-way repeated measures ANOVA followed by Bonferroni post hoc test (**f**, **g**, **i**). The data represent three independent experiments with similar results. Source data are provided as a Source Data file.

downstream processing. The processed data of sc/snRNA-seq were imported using the anndata package (0.7.5.6)[53,54]. Doublets were identified using scDblFinder (1.6.0, Bioconductor, Buffalo, NY, USA) and subsequently removed. PKN gene was visualized expression using Seurat's feature plot feature[55].

### Isolation of adult murine cardiac fibroblast

C57BL/6 mice were anesthetized with hydrochloric acid medetomidine (0.3 mg/kg), midazolam (4 mg/kg), and butorphanol tartrate (5 mg/kg)[56]. The chest was opened, and ethylenediaminetetraacetic acid (EDTA) buffer was injected into the right ventricle. Subsequently, the hearts were quickly removed and cannulated through the aorta using a blunted 24-gauge needle. They were connected to a perfusion apparatus for retrograde perfusion of the coronary arteries with EDTA buffer and collagenase buffer (type II and IV collagenase: Worthington; protease XIV: Sigma-Aldrich). The ventricles were gently separated into small pieces with forceps and dissociated by pipetting. Cells were passed through a 100-μm strainer and left to settle for 20 min. The supernatant was collected and cultured in DMEM F12 supplemented with 10% FBS. The cultured cells were evaluated using immunofluorescence staining with a combination of the following antibodies: PDGFRα, CD31, CD45, and DAPI. We confirmed that 92–98% were PDGFRα-positive cells (well number = 4, counted cells ≥135/well). One-passage murine cardiac fibroblasts were used for all experiments.

### Immunoblot analysis

Western blotting was conducted to detect specific proteins. Protein extracts from cells and tissues were prepared by lysis in a radioimmunoprecipitation assay buffer (Wako, Osaka, Japan) containing protease inhibitor and phosphatase inhibitor mixtures (Roche, Mannheim, Germany). The protein concentration was measured using a BCA protein assay (Thermo Fisher Scientific, Waltham, MA, USA). Equal amounts of proteins were separated using sodium dodecyl sulfate-polyacrylamide gel electrophoresis and transferred onto a PVDF membrane. An ECL prime western blotting detection reagent (Cytiva, Tokyo, Japan) was used to detect signals. Relative phosphorylation and protein levels were quantified using ImageJ (National Institutes of Health, Bethesda, MD, USA).

### mRNA expression analysis

RNA was extracted from adult murine cardiac fibroblast and the left ventricle using the RNeasy Mini kit or RNeasy Plus Micro kit (Qiagen, Hilden, Germany) and reverse-transcribed using the ReverTraAce qPCR RT Master Mix (Toyobo, Osaka, Japan)[23]. Quantification was performed using the TB Green Premix Ex Taq II (Takara Bio, Tokyo, Japan). To analyze the absolute copy numbers of *Pkn1*, *Pkn2*, and *Pkn3*, we extracted genomic DNA from mouse tails and used it as a universal standard to calculate the copy number of genes[23]. The PCR primer sequence of *Pkn1*, *Pkn2*, and *Pkn3* were as follows: *Pkn1*, 5′-CTT CGA TGA GGA GTT CAC TGG-3′, 5′-CGG CCA CAA AGT CGA AAT-3′; *Pkn2*, 5′-AGA AAT AAG GAA AGA ACT GAA AAT CAA-3′, 5′- GCC AAA TTT TTC TTA TCT GTT GTA ACT-3′; and *Pkn3*, 5′- AGA AGC TGG ACC TCC TAC GG-3′, 5′-TTC TTG GGT CAC CCT GCT AC-3′. The PCR primer sequence of *Col1* and *Col3* were as follows: *Col1a1* 5′-CCT GCT GGT GAG AAA GGA TCT-3′, 5′-GGA AGA CCA GGG AAG CCT CT-3′; *Col3a1* 5′-CTC CTG GTC TGC AAG GGA TG-3′, 5′-TTT CCT GGA ACT CCG TCA GC-3′; and *Rps18* 5′-TTC TGG CCA ACG GTC TAG ACA AC-3′, 5′-CCA GTG GTC TTG GTG TGC TGA-3′. Data were presented after normalization to Rps18 expression.

### siRNA transfections

Isolated and cultured cardiac fibroblasts were transfected with siRNA (Sigma-Aldrich) and RNAiMAX (Invitrogen, Carlsbad, CA, USA) 24 h and 48 h after seeding following the manufacturer's instructions. The MISSION siRNAs (Sigma-Aldrich) used were mouse PKN1 (SASI_Mm01_00028143), mouse PKN2 (SASI_Mm01_00157604), and Universal Negative Control #1 (SIC001, Sigma-Aldrich).

### Virus vector transfections and treatments

Isolated and cultured cardiac fibroblasts were transfected with the GFP-PKN catalytic domain (CAT; VectorBuilder Inc., Chicago, USA) gene by lentivirus. After 24-h transfection, the fibroblasts were treated with SB203580, a p38 MAPK inhibitor (10 μM, Selleck, Houston, USA). After 48 h, the fibroblasts were evaluated with immunofluorescence staining.

### Cell proliferation assay

Isolated cardiac fibroblasts were treated with TGF-β (10 ng/mL, R&D Systems) and were transfected with siRNA twice after 48 h. The treated cells were evaluated using immunofluorescence staining with the combination of the antibodies αSMA, Ki67, and DAPI, and the number of cells with Ki67-positive nuclei were counted.

### Cell migration (wound healing assay)

Isolated cardiac fibroblasts were treated with TGF-β (10 ng/mL). After 48 h, they were transfected with siRNA twice. The treated cells were seeded with a 500-μm open gap using 2-well culture-inserts (ibidi GmbH, Graufelfing, Germany), and the migration of cells filling the damaged areas through the open gap was observed under a microscope for 12 h.

### Cell differentiation assay

At 24 h after the second siRNA transfection, cardiac fibroblasts were treated with TGF-β (10 ng/mL) for 48 h. The treated cells were evaluated using immunofluorescence staining with the combination of the antibodies αSMA, PDGFRα, and DAPI, and the number of αSMA-positive cells and PDGFRα-positive cells was counted.

### PKN1 and PKN2 knockout mice

Tamoxifen-inducible, cardiac fibroblast-specific PKN1- and PKN2-knockout (KO) mice models were generated by intercrossing the Pdgfra-Cre-ERT mice with *Pkn1*$^{flox/flox}$ and *Pkn2*$^{flox/flox}$ mice[23,29].

https://doi.org/10.1038/s41467-024-52068-0

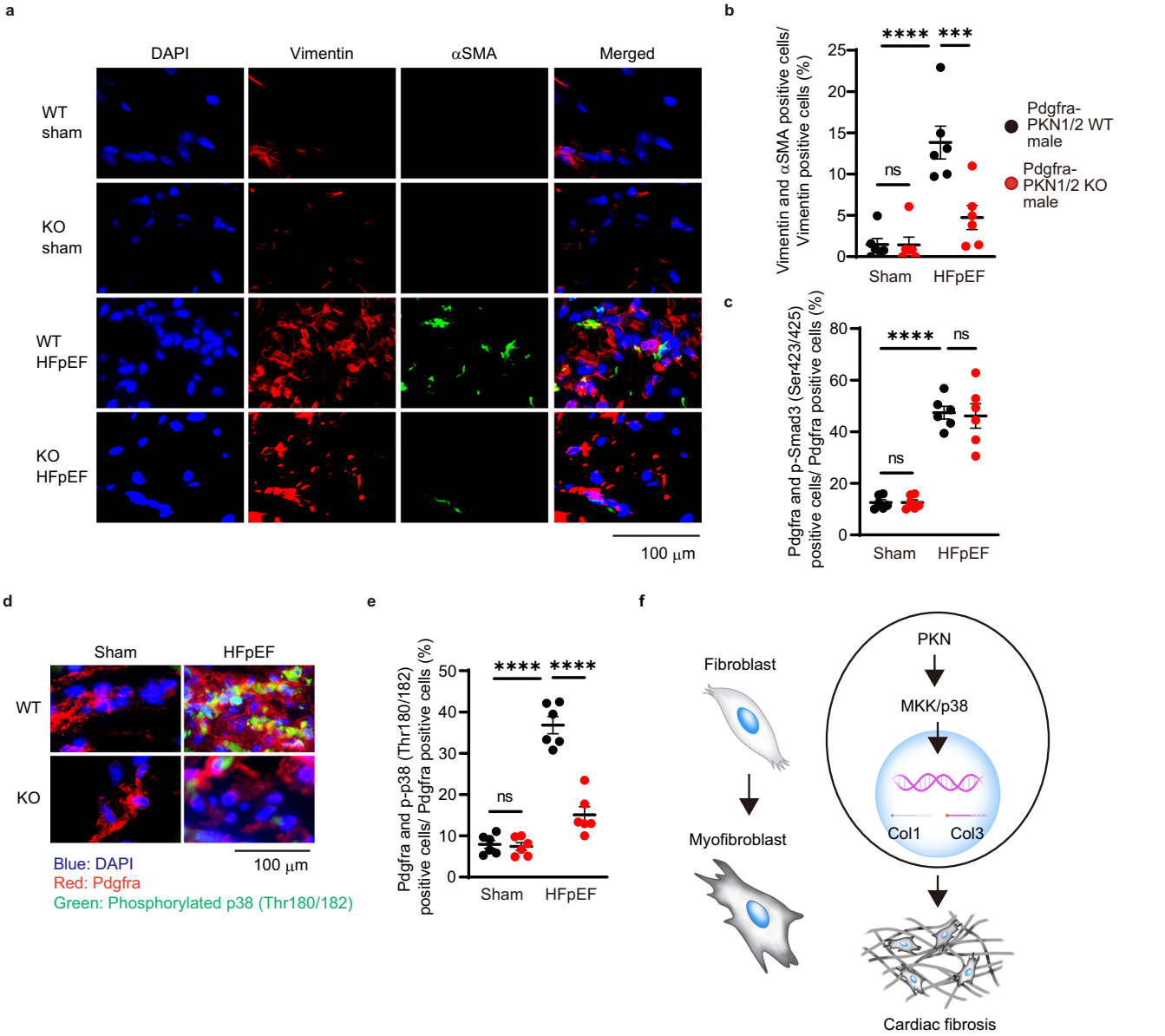


**Fig. 9 | PKN1/2 deletion suppressed the differentiation of cardiac fibroblasts in the HFpEF model. a** Immunofluorescent staining of fibroblasts and myofibroblasts at 10 weeks after combination exposure to HFD and L-NAME in Pdgfra-PKN1/2 WT and KO male mice (red, vimentin; green, αSMA; blue, nuclei). **b** Quantification of dual-positive cells for vimentin and αSMA shown as a percentage of vimentin-positive cells ($n = 6$, biological replicates per group). ns, not significant; ***$p = 0.0008$; ****$p < 0.0001$. **c** Quantification of the number of cardiac fibroblasts with phosphorylated Smad3 (Ser423/425) at 10 weeks after combination exposure to HFD and L-NAME in Pdgfra-PKN1/2 WT and KO male mice ($n = 6$, biological replicates per group). ns, not significant; ****$p < 0.0001$. Immunofluorescent images (**d**) and quantification of the number (**e**) of cardiac fibroblasts with phosphorylated p38 at 10 weeks after combination exposure to HFD and L-NAME in Pdgfra-PKN1/2 WT and KO male mice ($n = 6$, biological replicates per group. Red, Pdgfra; green, phosphorylated p38; blue, nuclei). ns, not significant; ****$p < 0.0001$. **f** Schematic diagram showing PKN1/2-mediated cardiac fibrosis. Data are presented as the mean ± SEM and analyzed using two-way ANOVA followed by the Tukey's post hoc test (**b**, **c**, **e**). The data represent three independent experiments with similar results. Source data are provided as a Source Data file.

Cardiomyocyte-specific PKN1- and PKN2-KO (cmc-PKN1/2 KO) mice have been reported previously[23]. Cre-mediated recombination of floxed alleles was induced by administering tamoxifen (1 mg) dissolved in 100 μL of Miglyol, through intraperitoneal injections for 5 days consecutively. Control animals (Pdgfra-Cre-ERT$^{+/-}$, *Pkn1*$^{wt/wt}$ and *Pkn2*$^{wt/wt}$ mice or αMHC-CreERT2$^{+/-}$, *Pkn1*$^{wt/wt}$ and *Pkn2*$^{wt/wt}$ mice) were also treated with tamoxifen. The experiments were performed 10 days after the end of induction.

All mice were bred at 20–22 °C and 50% relative humidity in a 12 h light/dark cycle. Mice were maintained in free access to water and standard chow (CE-2, CLEA Japan Inc., Tokyo, Japan). The mice were closely observed and sacrificed quickly, at a humane end point (no locomotion or body weight loss exceeding 20% of the initial body weight) using carbon dioxide inhalation.

## Animal model

A two-hit mouse model of HFpEF was assessed in 8- to 10-week-old Pdgfra-PKN1/2 WT and KO male and female mice and in 8- to 10-week-old cmc-PKN1/2 WT and KO male mice[38]. HFD and L-NAME (0.5 g l-1 in drinking water) treatments were administered for 10 weeks. We replenished HFD twice a week and L-NAME three times a week. IR injury was induced in 8- to 10-week-old Pdgfra-PKN1/2 WT and KO male mice[57]. The left anterior descending artery was transiently ligated with a 6-0 silk suture around PE-10 tubing with a

slipknot for 45 min. Then, continuous reperfusion was performed until echocardiography, and the mice were euthanized. The MI injury was performed by permanently ligating the left anterior descending artery.

Eight-week-old Pdgfra-PKN1/2 WT and KO male mice were anesthetized, and osmotic minipumps (Alzet model 2004; Alzet, Cupertino, CA) containing a physiological salt solution with or without angiotensin II (AngII; 100 $ng \cdot g^{-1} \cdot d^{-1}$, Sigma-Aldrich) were implanted subcutaneously in the back where they remained for 4 weeks. Osmotic minipumps were primed in sterile saline solution at 37 °C for 24 h before implantation.

Echocardiography with a Vevo 1100 (Fujifilm Visualsonics, Bothell, WA) was performed to assess cardiac function. The LV systolic function (%FS) was assessed in the short-axis M-mode view at the level of the midpapillary muscles. Apical four-chamber images were obtained for diastolic function measurements using pulsed-wave and tissue Doppler imaging at the mitral valve level in mice anesthetized with 1.0–1.5% isoflurane and adjusted to maintain a heart rate within the range of 450 beats/min to 550 beats/min.

An apical approach was used to obtain invasive pressure-volume measurements from anesthetized (1.0–1.5% isoflurane) mice using a Millar catheter (SPR 839, Millar Instruments, Inc, Houston, TX, USA)[58]. The inferior vena cava was occluded to acquire EDPVR. Data analysis was conducted using LabChart 7 (ADInstruments Pty Ltd., Bella Vista, Australia). Frozen mouse heart samples were embedded in an OCT compound (Sakura Finetek, Tokyo, Japan) and prepared for histological analysis. Fibrosis was assessed through Picrosirius red staining after 4 weeks of AngII treatment, 7 and 28 days after IR injury, or after 10 weeks of exposure to L-NAME and HFD. The average area of interstitial fibrosis was evaluated at the cross-section of the left ventricle in IR or in 12 random locations in HFpEF and AngII-induced heart failure, using Image J.

### Immunofluorescence staining

Cells and sections for immunofluorescence staining were washed thoroughly in phosphate-buffered saline (PBS) and fixed with 4% paraformaldehyde for 15 min. Subsequently, 0.5% Triton X-100 in PBS was applied for 10 min, and the samples were blocked in Protein Block Serum-Free (Agilent Technologies, Santa Clara, CA, USA) for 10 min. Afterward, they were incubated with primary antibodies diluted in 1% PBS at 4 °C overnight. The sections were then incubated with secondary antibodies (Alexa Fluor 488 and 647; Thermo Fisher Scientific, Waltham, MA, USA) for 1 h. Nuclei were counterstained using Cellstain DAPI Solution. Images were taken using a BZ-X microscope (KEYENCE, Osaka, Japan).

### Statistical analysis

Trial experiments or experiments performed previously were used to determine the appropriate sample size with adequate statistical power. The investigator was blinded to group allocation during the experiment. Data are presented as the mean ± SEM in all experiments. All statistical analyses for animal experiments were performed using GraphPad Prism 9 (GraphPad Software Inc., San Diego, CA, USA). Data were analyzed using a two-sided unpaired Student *t* test to compare means for the two experimental groups. Meanwhile, two-way analysis of variance (ANOVA) with Tukey's post hoc test or two-way repeated measures ANOVA with Bonferroni post hoc testing was used to compare two or more independent variables. "n" refers to the number of independent experiments or mice per group. Significance was defined as $p < 0.05$.

### Reporting summary

Further information on research design is available in the Nature Portfolio Reporting Summary linked to this article.

## Data availability

All data are available in the main text or the supplementary materials. Source data are provided within this paper. PKN expression in cardiac cells was analyzed using a publicly available dataset from the Heart Cell Atlas (Source: https://www.heartcellatlas.org/)[26]. Source data are provided with this paper.

## References


1. Wynn, T. A. Cellular and molecular mechanisms of fibrosis. *J. Pathol.* **214**, 199–210 (2008).
2. Wijsenbeek, M., Suzuki, A. & Maher, T. M. Interstitial lung diseases. *Lancet* **400**, 769–786 (2022).
3. Ginès, P. et al. Liver cirrhosis. *Lancet* **398**, 1359–1376 (2021).
4. Henderson, N. C., Rieder, F. & Wynn, T. A. Fibrosis: from mechanisms to medicines. *Nature* **587**, 555–566 (2020).
5. Savarese, G. & Lund, L. H. Global public health burden of heart failure. *Card. Fail. Rev.* **3**, 7–11 (2017).
6. Schelbert, E. B. et al. Myocardial fibrosis quantified by extracellular volume is associated with subsequent hospitalization for heart failure, death, or both across the spectrum of ejection fraction and heart failure stage. *J. Am. Heart Assoc.* **4**. https://doi.org/10.1161/jaha.115.002613 (2015).
7. González, A., Schelbert, E. B., Díez, J. & Butler, J. Myocardial interstitial fibrosis in heart failure: biological and translational perspectives. *J. Am. Coll. Cardiol.* **71**, 1696–1706 (2018).
8. Tarbit, E., Singh, I., Peart, J. N. & Rose'Meyer, R. B. Biomarkers for the identification of cardiac fibroblast and myofibroblast cells. *Heart Fail. Rev.* **24**, 1–15 (2019).
9. Talman, V. & Ruskoaho, H. Cardiac fibrosis in myocardial infarction-from repair and remodeling to regeneration. *Cell Tissue Res.* **365**, 563–581 (2016).
10. Owan, T. E. et al. Trends in prevalence and outcome of heart failure with preserved ejection fraction. *N Engl J. Med.* **355**, 251–259 (2006).
11. Mohammed, S. F. et al. Coronary microvascular rarefaction and myocardial fibrosis in heart failure with preserved ejection fraction. *Circulation* **131**, 550–559 (2015).
12. Redfield, M. M. & Borlaug, B. A. Heart failure with preserved ejection fraction: a review. *JAMA* **329**, 827–838 (2023).
13. Tallquist, M. D. Cardiac fibroblast diversity. *Annu. Rev. Physiol.* **82**, 63–78 (2020).
14. Wei, K., Nguyen, H. N. & Brenner, M. B. Fibroblast pathology in inflammatory diseases. *J. Clin. Investig.* **131**. https://doi.org/10.1172/jci149538 (2021).
15. Tallquist, M. D. & Molkentin, J. D. Redefining the identity of cardiac fibroblasts. *Nat. Rev. Cardiol.* **14**, 484–491 (2017).
16. Meng, X. M., Nikolic-Paterson, D. J. & Lan, H. Y. TGF-β: the master regulator of fibrosis. *Nat. Rev. Nephrol.* **12**, 325–338 (2016).
17. Bretherton, R., Bugg, D., Olszewski, E. & Davis, J. Regulators of cardiac fibroblast cell state. *Matrix Biol* **91-92**, 117–135 (2020).
18. Amano, M. et al. Identification of a putative target for Rho as the serine-threonine kinase protein kinase N. *Science* **271**, 648–650 (1996).
19. Watanabe, G. et al. Protein kinase N (PKN) and PKN-related protein rhophilin as targets of small GTPase Rho. *Science* **271**, 645–648 (1996).
20. Manning, G., Whyte, D. B., Martinez, R., Hunter, T. & Sudarsanam, S. The protein kinase complement of the human genome. *Science* **298**, 1912–1934 (2002).
21. Shimokawa, H., Sunamura, S. & Satoh, K. RhoA/Rho-Kinase in the Cardiovascular System. *Circ. Res.* **118**, 352–366 (2016).
22. Jin, Y. J. et al. Protein kinase N2 mediates flow-induced endothelial NOS activation and vascular tone regulation. *J. Clin. Investig.* **131**. https://doi.org/10.1172/jci145734 (2021).

23. Sakaguchi, T. et al. Protein Kinase N promotes stress-induced cardiac dysfunction through phosphorylation of myocardin-related transcription factor A and disruption of its interaction with actin. *Circulation* **140**, 1737–1752 (2019).
24. Murray, E. R. et al. Disruption of pancreatic stellate cell myofibroblast phenotype promotes pancreatic tumor invasion. *Cell Rep.* **38**, 110227 (2022).
25. Thumkeo, D., Watanabe, S. & Narumiya, S. Physiological roles of Rho and Rho effectors in mammals. *Eur. J. Cell Biol.* **92**, 303–315 (2013).
26. Kanemaru, K. et al. Spatially resolved multiomics of human cardiac niches. *Nature* **619**, 801–810 (2023).
27. Flynn, P., Mellor, H., Casamassima, A. & Parker, P. J. Rho GTPase control of protein kinase C-related protein kinase activation by 3-phosphoinositide-dependent protein kinase. *J. Biol. Chem.* **275**, 11064–11070 (2000).
28. Dong, L. Q. et al. Phosphorylation of protein kinase N by phosphoinositide-dependent protein kinase-1 mediates insulin signals to the actin cytoskeleton. *Proc. Natl Acad. Sci. USA* **97**, 5089–5094 (2000).
29. Miwa, H. & Era, T. Generation and characterization of PDGFRα-GFPCreERT2 knock-In mouse line. *Genesis* **53**, 329–336 (2015).
30. Ma, Y., Iyer, R. P., Jung, M., Czubryt, M. P. & Lindsey, M. L. Cardiac fibroblast activation post-myocardial infarction: current knowledge gaps. *Trends Pharmacol. Sci.* **38**, 448–458 (2017).
31. Frangogiannis, N. Transforming growth factor-β in tissue fibrosis. *J. Exp. Med.* **217**, e20190103 (2020).
32. Frangogiannis, N. G. Cardiac fibrosis. *Cardiovasc. Res.* **117**, 1450–1488 (2021).
33. Rudat, C., Norden, J., Taketo, M. M. & Kispert, A. Epicardial function of canonical Wnt-, Hedgehog-, Fgfr1/2-, and Pdgfra-signalling. *Cardiovasc. Res.* **100**, 411–421 (2013).
34. Molkentin, J. D. et al. Fibroblast-specific genetic manipulation of p38 mitogen-activated protein kinase in vivo reveals its central regulatory role in fibrosis. *Circulation* **136**, 549–561 (2017).
35. Derynck, R. & Zhang, Y. E. Smad-dependent and Smad-independent pathways in TGF-beta family signalling. *Nature* **425**, 577–584 (2003).
36. Corre, I., Paris, F. & Huot, J. The p38 pathway, a major pleiotropic cascade that transduces stress and metastatic signals in endothelial cells. *Oncotarget* **8**, 55684–55714 (2017).
37. Westermann, D. et al. Cardiac inflammation contributes to changes in the extracellular matrix in patients with heart failure and normal ejection fraction. *Circ. Heart Fail.* **4**, 44–52 (2011).
38. Schiattarella, G. G. et al. Nitrosative stress drives heart failure with preserved ejection fraction. *Nature* **568**, 351–356 (2019).
39. Jacques, D. C., Pinsky, M. R., Severyn, D. & Gorcsan, J. 3rd Influence of alterations in loading on mitral annular velocity by tissue Doppler echocardiography and its associated ability to predict filling pressures. *Chest* **126**, 1910–1918 (2004).
40. Ogilvie, L. M. et al. Hemodynamic assessment of diastolic function for experimental models. *Am. J. Physiol. Heart Circ. Physiol.* **318**, H1139–h1158 (2020).
41. Lam, C. S. P. et al. Sex differences in heart failure. *Eur. Heart J.* **40**, 3859–3868c (2019).
42. Roskoski, R. Jr. Properties of FDA-approved small molecule protein kinase inhibitors: A 2023 update. *Pharmacol. Res.* **187**, 106552 (2023).
43. Frangogiannis, N. G. Cardiac fibrosis: cell biological mechanisms, molecular pathways and therapeutic opportunities. *Mol. Aspects Med.* **65**, 70–99 (2019).
44. Fu, X. et al. Specialized fibroblast differentiated states underlie scar formation in the infarcted mouse heart. *J. Clin. Investig.* **128**, 2127–2143 (2018).
45. Shah, S. J. et al. Phenotype-specific treatment of heart failure with preserved ejection fraction: a multiorgan roadmap. *Circulation* **134**, 73–90 (2016).
46. Lam, C. S. P., Voors, A. A., de Boer, R. A., Solomon, S. D. & van Veldhuisen, D. J. Heart failure with preserved ejection fraction: from mechanisms to therapies. *Eur. Heart J.* **39**, 2780–2792 (2018).
47. Zile, M. R. et al. Myocardial stiffness in patients with heart failure and a preserved ejection fraction: contributions of collagen and titin. *Circulation* **131**, 1247–1259 (2015).
48. Tong, D. et al. Female sex is protective in a preclinical model of heart failure with preserved ejection fraction. *Circulation* **140**, 1769–1771 (2019).
49. Villalobos, E. et al. Fibroblast primary cilia are required for cardiac fibrosis. *Circulation* **139**, 2342–2357 (2019).
50. Kong, P. et al. Opposing actions of fibroblast and cardiomyocyte Smad3 signaling in the infarcted myocardium. *Circulation* **137**, 707–724 (2018).
51. Doza, Y. N., Cuenda, A., Thomas, G. M., Cohen, P. & Nebreda, A. R. Activation of the MAP kinase homologue RK requires the phosphorylation of Thr-180 and Tyr-182 and both residues are phosphorylated in chemically stressed KB cells. *FEBS Lett.* **364**, 223–228 (1995).
52. Chang, L. & Karin, M. Mammalian MAP kinase signalling cascades. *Nature* **410**, 37–40 (2001).
53. Hao, Y. et al. Integrated analysis of multimodal single-cell data. *Cell* **184**, 3573–3587.e3529 (2021).
54. Wolf, F. A., Angerer, P. & Theis, F. J. SCANPY: large-scale single-cell gene expression data analysis. *Genome Biol.* **19**, 15 (2018).
55. Germain, P. L., Lun, A., Garcia Meixide, C., Macnair, W. & Robinson, M. D. Doublet identification in single-cell sequencing data using scDblFinder. *F1000Res* **10**, 979 (2021).
56. Ishihama, S. et al. LPL/AQP7/GPD2 promotes glycerol metabolism under hypoxia and prevents cardiac dysfunction during ischemia. *FASEB J.* **35**, e22048 (2021).
57. Fan, Q. et al. Dectin-1 Contributes to myocardial ischemia/reperfusion injury by regulating macrophage polarization and neutrophil infiltration. *Circulation* **139**, 663–678 (2019).
58. Pacher, P., Nagayama, T., Mukhopadhyay, P., Bátkai, S. & Kass, D. A. Measurement of cardiac function using pressure-volume conductance catheter technique in mice and rats. *Nat. Protoc.* **3**, 1422–1434 (2008).


## Acknowledgements

We thank the staff of the Division of Experimental Animals at the Nagoya University School of Medicine for assisting in animal experiments. This work was supported by the Japan Society for the Promotion of Science KAKENHI (23H02903) and by the Hori Sciences and Arts Foundation (M.T.). All images of Fig. 9f were prepared as original elements created by Medical Illust Niia (Kanagawa, Japan).

## Author contributions

S.Y. performed most of the in vitro and in vivo experiments, analyzed, and discussed data, and commented on the manuscript. T.Y., K.I., and T.H. performed in vivo experiments and mouse generation. Y.Y. and K.K. performed phosphorylation experiments. A.E., K.O., N.O., N.W., S.O., and T.M. initiated and supervised the study, discussed data, and commented on the manuscript. T.O. and H.K. supervised the study and commented on the manuscript. M.T. initiated the study, performed in vitro and in vivo experiments, analyzed and discussed data, and wrote the manuscript. Correspondence and requests for materials should be addressed to M.T.

## Competing interests

The authors declare no competing interests.

## Additional information

**Supplementary information** The online version contains supplementary material available at https://doi.org/10.1038/s41467-024-52068-0.

**Correspondence** and requests for materials should be addressed to Mikito Takefuji.

**Peer review information** *Nature Communications* thanks Hind Lal, Joshua Hare, and the other, anonymous, reviewer(s) for their contribution to the peer review of this work. A peer review file is available.